Pergamon

Int. J. Heat Mass Transfer. Vol. 39, No. 8, pp. 1569–1583, 1996

0017–9310/96 $15.00+0.00

0017–9310(95)00263–4

Theoretical analysis for axisymmetric mixed convection between rotating coaxial disks

C. Y. SOONG

Department of Aeronautical Engineering, Chung Cheng Institute of Technology, Tahsi, Taoyuan, Taiwan 33509, Republic of China

(*Received* 19 *January* 1995 *and in final form* 10 *July* 1995)

Abstract—This paper deals with a similarity analysis of axisymmetric mixed convection between two horizontal infinite coaxial disks. Governing equations with respect to a rotating frame of reference are formulated, and Boussinesq approximation is invoked to explore centrifugal-buoyancy effects. The rotational conditions of two disks rotating at different rates are mainly concerned. Upon considering Reynolds number up to 2000 and the buoyancy parameter ($B = \beta\Delta T$) of $|B| \leqslant 0.1$, the rotational effects on the flow and heat transfer characteristics are examined. Analytic features of the high-Re solution behaviors are also studied. By using the present similarity model, flow structure patterns of co-rotating, counter-rotating and rotor–stator systems under the influence of buoyancy effect are disclosed. Furthermore, the results also reveal the significance of centrifugal buoyancy in flow and heat transfer characteristics. For co-rotating disks, the centrifugal-buoyancy effects are reflected in the velocity field and skin friction. In the case of counter-rotating disks, remarkable buoyancy effects exert on the temperature field, heat transfer rate, and the radial skin friction. For rotor–stator systems, the buoyancy effects on boundary derivatives are insignificant, while those on core-flow in high-Re cases are noticeable.

INTRODUCTION

Rotating-disk flow has long been an important topic in fluid dynamic research for the interests in practical as well as academic senses. After the similarity analysis for the free-disk flow proposed by von Karman [1], numerous investigations have also been carried out for the flow fields associated with either single-disk or two coaxial disks. Batchelor [2] extended von Karman's analysis to explore the two-disk flow. By examining the qualitative nature rather than actually solving the governing equations, he proposed flow structure models for two-disk problems. Later on, based on the series solutions at low Reynolds numbers and the experimental observations, Stewartson [3] challenged Batchelor's conjecture. A number of investigations [4–8] were carried out for better understanding of this class of rotating flows. Mathematically, the problem becomes very stiff at high Reynolds number, it leads to some difficulties in numerical calculations. Therefore, some previous investigations focused on the development of numerical techniques for high Reynolds number solutions, e.g. the continuation method by Roberts and Shipman [9] and the *ad hoc* difference scheme by Barrett [10].

By considering the non-uniformity of the fluid temperature, the non-isothermal flow in a rotating device may encounter a buoyancy effect in the presence of centrifugal force. The centrifugal buoyancy has been considered in some previous studies on rotating devices, e.g. the rotating closed cylinders [11–15], gas centrifuges [16, 17] and radially rotating channels [18–20]. Recently, mixed convection in rotating disk systems with a radial through-flow was studied by solutions of boundary-layer equations [21, 22] and Navier–Stokes equations [23]. For infinite coaxial disks without through-flow, Hudson [24] and Chew [25] have performed analyses for the non-isothermal flows between two co-rotating disks at the same rate. In the former, the problem was restricted to the low Reynolds number ($Re \leqslant 100$) and very small thermal Rossby number ($\beta\Delta T < 0.01$). While in the latter, Chew developed a linearized model by neglecting radial viscous terms and nonlinear inertia terms in momentum equations. However, the solution was essentially a highly simplified one.

In summary, as mentioned above, most of the previous investigations on thermal effects concentrated their attention on the flow between two co-rotating disks at the same rate only. Most recently, a study on time-dependent non-isothermal flows in two-disk systems has been performed by Soong and Ma [26]. However, the work mainly concerned the unsteadiness of the system. It seems evident that after more than forty years of research in this field, there are still many interesting questions that remain open in the two-disk problems. The significance and influences of the centrifugal buoyancy in non-corotating systems (two disks rotating at different rates and/or different senses) have not been reported yet.

Non-isothermal flows between two parallel infinite disks at various rotational conditions are considered in the present study, and the objective is to develop an axisymmetric model for the free, forced, and mixed

NOMENCLATURE

B	buoyancy parameter or thermal Rossby number, $\beta\Delta T$
C_f	skin friction coefficient, $2\mu(\partial U/\partial Z)_w/[\rho(R\Omega_1)^2]$
c_p	constant-pressure specific heat
$\mathbf{e}_r$, $\mathbf{e}_z$	unit vectors in radial and axial directions
$F(\eta)$	radial velocity function, $U/R\Omega_1$
Fr	Froude number, $S\Omega_1^2/g$
$G(\eta)$	tangential velocity function, $V/R\Omega_1$
g	gravitational acceleration (9.81 m s^2)
Gr	Grashof number, $(S\Omega_1^2)\beta\Delta TS^3/\nu^2$
$H(\eta)$	axial velocity function, $W/(\nu\Omega_1)^{1/2}$
K_1, K_2, K_3	parameters in equation (19)
Nu	Nusselt number, $-(\partial T/\partial n)_w/(T_2-T_1)$
P	static pressure
P^*	dimensional pressure departure from the reference state, $P^* = P-P_r$
Pr	Prandtl number, ν/α
R, φ, Z	cylindrical coordinates
R_o	outer radius of finite disk
Re	Reynolds number, $\Omega_1 S^2/\nu$
Re^*	local Reynolds number, $(R\Omega_1)S/\nu$
Re_t	tip Reynolds number for finite disks, $\Omega R_0^2/\nu$
Ri	Richardson number, Gr/Re^2
S	spacing between two coaxial disks
T	temperature
ΔT	characteristic temperature difference
U, V, W	velocity components in R–φ–Z coordinate system
$\mathbf{V}$	velocity vector, (U, V, W).

Greek symbols

α	thermal diffusivity, $k/\rho c_p$
β	thermal expansion coefficient, $-(1/\rho_r)(\partial\rho/\partial T)$
δ_E	Ekman layer thickness for location of peak value in F-distribution
δ_T	thermal boundary-layer thickness for location of $\theta = 0.999$
γ	dimensionless relative rotation rate of disk 2, $(\Omega_2-\Omega_1)/\Omega_1$
η	dimensionless axial coordinate, Z/S
$\theta(\eta)$	dimensionless temperature difference $(T-T_1)/\Delta T$
μ	dynamic viscosity
ν	kinematic viscosity
ξ	stretched coordinate, $Re^{1/2}\eta$
ζ	transformed coordinate, $\zeta = 1-\eta$
ϕ	dimensionless pressure, $P^*/\rho_r(S\Omega_1)^2$
ρ	density
Ω	rotational speed.

Superscript

$(\hat{})$	conjugate state
$(\,)'$	derivative, $\mathrm{d}(\,)/\mathrm{d}\eta$.

Subscripts

1	first disk
2	second disk
c	core
r	reference
t	tangential
Ω	rotation.

convection flow and heat transfer. In the case of two disks rotating at the same rate ($\Omega_2 = \Omega_1$), the co-rotation of the disks leads the isothermal flow to a solid-body rotation as well as heat-conduction state and, with respect to a rotating frame attached to the system, the velocity vector $\mathbf{V}$ in this case is null. But centrifugal force in the presence of non-uniform temperature field may result a buoyancy-induced flow, which is a pure free-convection in nature. For two disks rotating at different rates ($\Omega_2 \neq \Omega_1$), however, even though the fluid is isothermal the radial and axial flows can be driven by the unbalanced Coriolis-induced pumping effects near the two disks. In the absence of other forced flow source, this can be regarded as the forced-flow in rotating disk systems. By additionally considering the density variation in centrifugal force term, the buoyancy effect can be accounted for. Since both forced and free convection flows are caused by the same factor, the disk rotation, the flow and heat transfer mechanisms are quite different from that in conventional mixed convection with gravity as the only body force.

To take into account the density variation in centrifugal force term, Boussinesq approximation is invoked in the study. It has been demonstrated that the isothermal wall is the only possible thermal boundary condition for similarity transformation of rotating-disk problems [27]. By using the von Karman's hypothesis on velocity variables and proposing a properly-defined temperature function, the similarity equations can be formulated under the assumptions of axisymmetric flow and infinitely large disks. For very large tip Reynolds number $Re_t(=\Omega R_0^2/\nu)$ in finite disk systems, say $Re_t \sim O(10^5)$ or higher, the flows may become turbulent in nature [28], and rotating stall phenomenon [29] may appear. However, the flows still have the chance to be laminar and stall-free for lower Re_t. In another respect, a similarity model is very useful in the study of some fundamental natures in rotating-disk flows. These class of theoretical analy-

ses have been used in considerable number of studies, such as refs. [1–6, 12, 13, 23, 24] for steady rotating-disk flows, Stewartson *et al.* [30], Singh *et al.* [31] and Soong and Ma [26] for unsteady rotating-disk flows, Higgins [32] and Rehg and Higgins [33] for film flow on rotating-disk, to name only a few. By using the similarity model developed presently, three situations of rotation: (1) two disks rotating in the same sense (*co-rotating disks*), (2) rotating in opposed senses (*counter-rotating disks*) and (3) one disk rotating and another one at rest (for brevity, hereafter, the system is referred to as *rotor–stator*) are studied. The analytic features of the present similarity solutions, i.e. asymptotic natures of the high-Re solutions including the Ekman and thermal boundary layers, and the core flow behaviors are addressed. For wider ranges of the parameters, numerical integrations are employed in exploring the flow and heat transfer characteristics.

THEORETICAL ANALYSIS

Problem statement and formulation

The flow configuration considered, as in Fig. 1, is a system of two horizontal infinite coaxial disks separated by a spacing S. The disks are of constant temperatures T_1 and T_2, and rotate at rotational rates Ω_1 and Ω_2, respectively. A cylindrical coordinate (R, φ, Z) is fixed on the disk 1 and its origin lies at the disk center. With respect to the rotating frame of reference, Coriolis and centrifugal forces appear explicitly in the momentum equation. The fluid flow is assumed to be steady, laminar, axi-symmetric and of constant-property; and Boussinesq approximation is invoked for study of the centrifugal buoyancy effects. For simplicity, viscous dissipation and compression work are both ignored. The velocity components in R, φ and Z directions are U, V and W, respectively. In the present study, the wall condition of disk 1 is used as the reference state, at which the fluid confined by the disks lies at the temperature $T_r = T_1$ and rotates with the reference frame as a solid body, therefore, $U = V = W \equiv 0$ and $-\nabla P_r/\rho_r = \boldsymbol{\Omega}\times\boldsymbol{\Omega}\times\mathbf{R}+g$. Furthermore, by considering a linear density-temperature relation, $\rho = \rho_r[1-\beta(T-T_r)]$, the governing equations can be depicted as a similar form in the work of Homsy and Hudson [13]:

$$\nabla\cdot\mathbf{V} = 0 \tag{1}$$

$$(\mathbf{V}\cdot\nabla)\mathbf{V}+2\Omega_1(\mathbf{e}_z\times\mathbf{V})+\Omega_1^2 R\beta(T-T_r)\mathbf{e}_r - g\beta(T-T_r)\mathbf{e}_z = -\nabla P^*/\rho_r+\nu\nabla^2\mathbf{V} \tag{2}$$

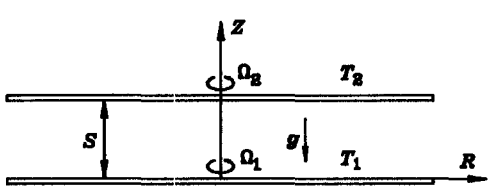

Fig. 1. Model of co-axially rotating infinite disk system.

$$(\mathbf{V}\cdot\nabla)T = \alpha\nabla^2 T \tag{3}$$

in which $P^* = P-P_r$ is the pressure departure from the reference condition, $\boldsymbol{\Omega} = \Omega_1\mathbf{e}_r$, $\mathbf{R} = R\mathbf{e}_r$, and $\mathbf{e}_z$ and $\mathbf{e}_r$ are the unit vectors in the axial and radial directions, respectively.

In the present analysis, the following dimensionless variables and parameters are used,

$$F(\eta) = U(R,Z)/R\Omega_1 \quad G(\eta) = V(R,Z)/R\Omega_1$$

$$H(\eta) = W(R,Z)/(\nu\Omega_1)^{1/2} \quad \theta(\eta) = [T(R,Z)-T_1]/\Delta T$$

$$\eta = Z/S \quad Re = S^2\Omega_1/\nu \quad B = \beta\Delta T \quad Pr = \nu/\alpha$$

where $\Delta T = T_2-T_1$ is the characteristic temperature difference. The transformation is essentially of von Karman-type but with an additional treatment to the temperature function and, therefore, the energy equation. The governing equations (1)–(3) can thus be cast into the following dimensionless form:

$$H'''' = Re^{1/2}HH''' - 4Re^{3/2}(1+G)G' - 2BRe^{3/2}\theta' \tag{4}$$

$$G'' = Re^{1/2}(HG'-H'G-H') \tag{5}$$

$$\theta'' = Pr\,Re^{1/2}H\theta' \tag{6}$$

in which the continuity equation,

$$H' = -2Re^{1/2}F \tag{7}$$

has been introduced to simplify the system by eliminating the radial velocity function $F(\eta)$. The superscript ( )′ denotes differentiation with respect to η, e.g. $H' = \mathrm{d}H/\mathrm{d}\eta$ and $G'' = \mathrm{d}^2G/\mathrm{d}\eta^2$. Equations (4) and (5), respectively, are the radial and circumferential components of the momentum equation (2). Upon defining a dimensionless pressure parameter $\phi \equiv P^*/\rho_r S^2\Omega_1^2$ and integrating Z component of the momentum equation, the pressure can be determined by

$$\phi = Re^{-3/2}H' - Re^{-1}H^2/2 - BFr^{-1}\theta, \tag{8}$$

where $Fr \equiv S\Omega_1^2/g$ is the rotational Froude number characterizing the ratio of centrifugal to gravitional forces. Considering a rapidly rotating system, the last term in (8) can be neglected for $Fr \gg 1$.

Boundary conditions

On the disks, according to the no-slip condition, the radial and axial velocities are zero. The tangential velocity G at the disk 1 is identically zero; however, due to relative motion of two disks, the tangential velocity at disk 2 is $R(\Omega_2-\Omega_1)$. Thermal boundary conditions at disk 1 and disk 2 are uniform wall temperatures T_1 and T_2, respectively. By defining a dimensionless rotation rate for disk 2, $\gamma \equiv (\Omega_2-\Omega_1)/\Omega_1$, the boundary conditions can be written as

$$H(0) = H'(0) = H(1) = H'(1) = 0$$

$$G(0) = G(1)-\gamma = 0$$

$$\theta(0) = \theta(1) - 1 = 0. \quad (9)$$

Note that the boundary conditions for $F(\eta)$, $F(0) = F(1) = 0$, have already been replaced by $H'(0) = H'(1) = 0$ through the relationship between $F(\eta)$ and $H'(\eta)$ in equation (7).

Governing parameters

There are five parameters involved in the problem considered, they are Pr, Re, B, γ, and Fr. In the present analysis, the Prandtl number Pr is 0.7 for air and the Froude number is assumed to be infinite. The Reynolds number Re and the buoyancy parameter B (in some literature, $\beta\Delta T$ was called thermal Rossby number) characterize rotational motion and centrifugal-buoyancy effects, respectively. The parameter γ denotes the relative rotation rate of the disk 2 with respect to the disk 1. For example, the values of $\gamma = 0$, -1 and -2 correspond to the cases of $\Omega_2 = \Omega_1$ (co-rotating disks), $\Omega_1 \neq \Omega_2 \equiv 0$ (rotor–stator), and $\Omega_2 = -\Omega_1$ (counter-rotating disks), respectively.

In the previous studies, e.g. refs. [2, 4, 5, 8], the parameter B was absent, and the only flow parameter was Re. By comparing with the mixed convection in gravitational force field, the roles of the parameters Re and B are similar to that played by the forced-flow and buoyancy parameters, respectively. Superficially, $B = \beta\Delta T$ is simply a thermal parameter and has nothing to do with rotation. In terms of the length scale S, velocity scale $S\Omega_1$ and replacing the gravity g by $S\Omega_1^2$, however, the parameter B is just equivalent to the form of the Richardson number in mixed convection in gravitational force field, i.e. $B \equiv \beta\Delta T = (S\Omega_1^2\beta\Delta T S^3/\nu^2)/(\Omega_1 S^2/\nu)^2 = \mathrm{Gr}/\mathrm{Re}^2 \equiv \mathrm{Ri}$, which characterizes the relative importance of buoyancy to the forced-flow in mixed convection problems. The zero thermal Rossby number, $B = \beta(T_2 - T_1) = 0$, indicates two possible buoyancy-free situations, i.e. $\beta = 0$ or $T_2 = T_1$. The former, $\beta = 0$, characterizes a forced-convection flow, in which buoyancy effect is ignored while the flow temperature nonuniformity and non-zero heat transfer are allowed. For the case of $T_2 = T_1$, no matter what $\theta(\eta)$-solution is, the uniform temperature profile of $T(\eta) \equiv T_1 = T_2$ can be shown from the definition of $\theta(\eta)$, i.e. $T(\eta) = T_1 + \theta(\eta)(T_2 - T_1)$. Therefore, the buoyancy effect and the heat transfer both are absent in this isothermal flow field.

Notice that, in the present flow configuration, Re can be used to characterize the forced flow as long as $\gamma \neq 0$ ($\Omega_1 \neq \Omega_2$). In the conventional free-convection study, $\beta\Delta T$ was usually small for the validity of Boussinesq approximation. For example, the magnitude less than 0.1 in the study of Gray and Giorgini [34] and, in a few cases, $\beta\Delta T \leqslant 0.2$ were used [35]. In the present study, the buoyancy parameter is restricted in the range of $|B| \leqslant 0.1$. The Reynolds number based on the disk spacing lies up to the magnitude of $O(10^3)$. The rotation parameter γ ranging from 0 to -2 is considered.

Definitions of friction factors and heat transfer rates

Based on the definition $C_f \equiv 2\mu(\partial U/\partial n)_w/[\rho(R\Omega_1)^2]$, where $(\partial U/\partial n)_w$ denotes the velocity gradient in normal direction to the walls, the radial friction factors at disks 1 and 2 are

$$C_{fr1}Re^* = 2F'(0) \quad C_{fr2}Re^* = -2F'(1), \quad (10)$$

respectively. Where $Re^* \equiv (R\Omega_1)S/\nu$ denotes the local Reynolds number. Similarly, the tangential friction factors are

$$C_{ft1}Re^* = 2G'(0) \quad C_{ft2}Re^* = -2G'(1). \quad (11)$$

The parameters $C_{ft1}Re^*$ and $C_{ft2}Re^*$ are closely related to the torque of the rotating disks. Heat transfer performance is expressed by Nusselt number defined as $Nu \equiv -(\partial T/\partial n)_w/(T_2 - T_1)$. By this definition the positive and negative values of Nu for $T_2 > T_1$ denote the heat transferred from and to the wall, respectively. For $T_2 < T_1$, the situation is reversed. The heat transfer rates on the two disks are

$$Nu_1 = -\theta'(0), Nu_2 = \theta'(1). \quad (12)$$

Asymptotic natures of solution behavior

In the past decades, numerous asymptotic analyses have been carried out to investigate the hydrodynamic natures in the limiting cases of high Reynolds numbers. The present mixed convection problem is more sophisticated for the coupling of flow and temperature fields. Before solving the coupled system, some characteristic features of the solution behavior for $Re \gg 1$ and $Pr \sim O(1)$ are examined analytically. By stretching the coordinate η with a factor of $Re^{1/2}$, i.e. $\xi = Re^{1/2}\eta$, equations (4)–(6) can be turned into the form:

$$H_{\xi\xi\xi\xi} = HH_{\xi\xi\xi} + 4(1+G)G_\xi - 2B\theta_\xi \quad (13)$$

$$G_{\xi\xi} = HG_\xi - H_\xi G - H_\xi \quad (14)$$

$$\theta_{\xi\xi} = PrH\theta_\xi, \quad (15)$$

where the variables with the subscript ξ denote their differentiations with respect to ξ. It demonstrates that the scales of Ekman and thermal boundary layers are of $O(Re^{-1/2})$, and the so-called inner-solution within the layers can be found by solving equations (13)–(15). Whereas the core solutions outside the layers are governed by the equations (4)–(6) for $Re \gg 1$. Upon dividing by $Re^{3/2}$, $Re^{1/2}$ and $Re^{1/2}$, respectively, equations (4)–(6) become

$$Re^{-3/2}H'''' = Re^{-1}HH''' + 4(1+G)G' - 2B\theta' \quad (4a)$$

$$Re^{-1/2}G'' = HG' - H'G - H' \quad (5a)$$

$$Re^{-1/2}\theta'' = Pr\,H\theta'. \quad (6a)$$

Taking a limit of $Re \to \infty$, results governing equations for core flows are:

$$2(1+G_c)G_c'-B\theta_c'=0 \quad (16)$$

$$H_cG_c'-H_c'(1+G_c)=0 \quad (17)$$

$$H_c\theta_c'=0, \quad (18)$$

where the variables G_c, H_c and θ_c stand for the core solutions or the outer-solutions in an asymptotic analysis. The possible solutions of (16)–(18) are:

(a) $\theta_c=K_1 \quad G_c=-1$ and H_c remains undetermined

(b) $\theta_c=K_1 \quad G_c=-1\pm\sqrt{(BK_1+K_2)}$ and $H_c=K_3(1+G_c)$

(c) $H_c=0 \quad G_c=-1\pm\sqrt{(B\theta_c+K_2)}$ and θ_c remains undetermined. (19)

In the above solutions, the parameters K_1, K_2 and K_3 and the undetermined solutions depend on the values of B and γ, and can be determined in the matching process of the inner and outer solutions for various values of B and γ. Among the solutions in equation (19), the solution (c) seems physically impossible, since the zero axial velocity in the core region, $H_c=0$, implies that there is no mutual communication between the fluids adjacent to the hot disk and the cold disk, and no interaction of wall-flow and the core-flow.

Analogous to the well-known layer-type (singular perturbation) problem: $\varepsilon\phi''-\phi\phi'-\phi=0$ with $\phi(0)=\phi_1$ and $\phi(1)=\phi_2$ [36], the solution behavior strongly depends on the boundary values ϕ_1 and ϕ_2. Therefore, the diversity of the self-similar solution can be expected for various values of the rotational parameter γ. For the complexities of the coupled system of nonlinear equations, there is no attempt herein to find the complete asymptotic solutions. Instead, the numerical solutions are used to explore the centrifugal-buoyancy effects at various conditions, while what was discussed in this section can be used to check and interpret the numerical solutions for high Re.

NUMERICAL PROCEDURE

The system of equations (4)–(6) with boundary conditions (9) consists of a nonlinear two-point boundary value problem. A typical shooting method can be started with the guessed missing conditions: $H''(0)=a$, $H'''(0)=b$, $G'(0)=c$ and $\theta'(0)=d$. In an iterative procedure, the values of a, b, c and d are updated by continuously using Newton's method until the boundary conditions at $\eta=1$, i.e. $H(1)=H'(1)=G(1)-\gamma=\theta(1)-1=0$, are met. The iteration is regarded as convergent if the stopping criterion, $\max(\Delta a, \Delta b, \Delta c, \Delta d)\leqslant 10^{-8}$ is satisfied. Low-Re solutions can be easily obtained using conventional shooting techniques. However, due to the stiffness of the system, the convergent solution is getting hard as Reynolds number increases. By applying non-uniform grid strategy, Aitkin acceleration technique, and the under-relaxation, the convergent solutions at high Reynolds numbers can be attained. A continuation concept is employed in the solution procedure, in which only one parameter, e.g. Re, B or γ, is changed case-by-case as the others are fixed. For example, by using the extrapolation of the solutions at Re, $Re+\Delta Re$, $Re+2\Delta Re$ as the initial guess for solutions at $Re+3\Delta Re$, the convergence characteristics of the iteration procedure can be improved. In the present nonlinear problem multiple solutions may exist for certain conditions. To make the solutions remain in the same branch, in the continuous computations, the change in the parameter should be small enough. The typical values of the small increments $\Delta Re=1$, $\Delta B=0.001$ and $\Delta\gamma=0.001$ were usually used. Through the numerical experiments, the grid-dependence of the numerical solutions were examined. For $Re\leqslant 500$, the grid of 201 points is sufficient for grid-independent solutions. For high Re, small $|\gamma|$, and/or large $|B|$, the finer grid, e.g. grid of 400 points or more, was used for either higher resolution and better convergence of the solutions. The symmetry nature of the two-disk flow solutions without considerations of heat transfer and centrifugal-buoyancy has been discussed by Keller and Szeto (K–S) [37]. An extension of the K–S lemma is developed for the present non-isothermal flows, and is stated in the Appendix. The analytic transformation for correspondence of the symmetric (or conjugate) solutions can be used to check the validity and the accuracy of the present numerical procedure.

RESULTS AND DISCUSSION

Comparisons of the similarity solutions with the finite-disk results

Except for the centrifugal buoyancy term, the present formulation differs from that in the previous works, e.g. ref. [4], for the different frames of reference used in the two studies. However, it is easy to verify that the two systems of equations are equivalent to each other under the buoyancy-free condition. Since the infinite-disk is an idealized flow configuration for theoretical analysis, the solutions can only be checked with the available finite-disk data. To the author's best knowledge, however, there is no measured data available on centrifugal-buoyancy in co-axially rotating disks. Figure 2 shows the comparisons of the present similarity solutions of rotor–stator ($\gamma=-1$) at $B=0$ with the Navier–Stokes computations [38] and the LDA measurements [39] on finite disks of the radius-to-spacing aspect ratio $R_o/S=10$. The agreement seems reasonable. In the previous studies [5, 6], it was claimed that the similarity structure can be retained in the inner region but broken down near the disk rim due to the presence of the edge effects. From the comparison in Fig. 2, obviously, the present similarity solutions appear reasonable for flow in partial region of the field, e.g. at least up to $R/R_o\simeq 0.6$ in

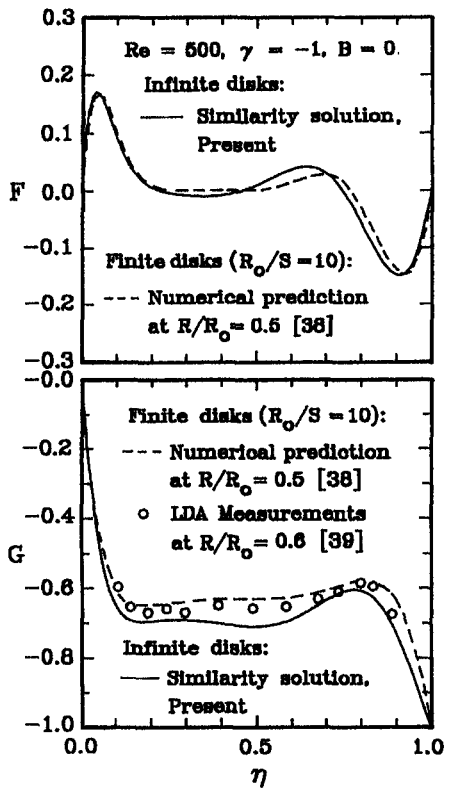

Fig. 2. Comparisons of the similarity solutions with the previous finite disk results.

this case. Similar consequence for flow in laminar regime of $Re_t = \Omega R_0^2/\nu = 1 \times 10^5$ can be found in the work of Itoh *et al.* [40].

Velocity and temperature fields

In the present work, the velocity and temperature fields at various rotational conditions, i.e. disks rotating in the same sense, in opposed senses, and as a rotor–stator system, are studied. For convenience, only the typical cases of $\Omega_2 = \Omega_1$ and $\Omega_2 = -\Omega_1$ are presented for co-rotating and counter-rotating disks, respectively. The case $\Omega_1 \neq \Omega_2 = 0$ is the only case of the rotor–stator and is certainly included in the following discussion.

Co-rotating disks with $\Omega_2 = \Omega_1$ ($\gamma = 0$). In buoyancy-free cases, the fluid rotates with the system as a solid body and without any flow in radial and axial directions. For $B = 0$ with arbitrary Re, the solutions are $F = G = H \equiv 0$ and $\theta \equiv \eta$. Consideration of the non-isothermal flow results in free-convection effect. In Fig. 3, buoyancy-induced flows at various Reynolds numbers and buoyancy parameters are shown, while the temperature solutions remain nearly as the conduction state.

In this pure free-convection situation, the fluid is pumped radially outward along the cooler disk and the incoming fluid is supplied by the inward sucked flow along the hotter disk. The flow in the near-wall regions is radially inward or outward depending upon the relative level of wall temperatures at the two disks. For $B > 0$, i.e. $T_2 > T_1$, the cooler fluid adjacent to the disk 1 can be pushed radially outward just like the results in Fig. 3(a). At the relatively higher Reynolds numbers, $Re > 100$, the bulk radial flow is confined in the thin layers near the rotating disks and a core region of slow-moving fluid forms. The rotational rate of the fluid changes only slightly, e.g. $G < 0.025$ at $Re = 300$. In this situation, the flow is still conduction-dominated and the temperature field lies not far from the conduction state. For $B < 0$ in Fig. 3(b) the flow direction is inverted due to the adverse effect of buoyancy.

Counter-rotating disks with $\Omega_2 = -\Omega_1$ ($\gamma = -2$). In case two disks rotate in opposite senses but at the same rate, due to the strong effects of rotation near the disk walls, the Coriolis effect pumps the fluid radially outward, the inward flow in the central region is induced for continuity. The incoming fluid in the core region approaches the two disks separately and forms a two-cell structure, of which the region between the dividing stream-surface (DSS, the plane of $H = 0$ parallel to the disks) and the disk 1 ($\eta = 0$) is cell 1 and that between DSS and disk 2 is cell 2. For buoyancy-free case, $B = 0$, the DSS locates at $\eta = 0.5$, while for $B > 0$ ($B < 0$), the two cells are of different strengths and the DSS at somewhere $\eta > 0.5$ ($\eta < 0.5$). As shown in Fig. 4(a) for relatively lower Reynolds number, $Re = 100$, the buoyancy effects on the velocity and temperature fields are remarkable. While for the higher Reynolds numbers, e.g. $Re = 500$ and 1000 in Figs. 4(b) and (c), the influences of the centrifugal-buoyancy on the tangential velocity G are diminished. Buoyancy effect on radial velocity F is still obvious in the thin Ekman layer but gradually alleviates in the core region.

It is noteworthy, however, that the temperature distribution is strongly affected by the buoyancy especially in the cases of high Re. For $B > 0$, comparing the solutions of $B = 0.1$ with that of $B = 0$ at $Re = 500$ in Fig. 4(b), it is found that the magnitudes of the radial and axial velocities both are increased in cell 1 region for $B = 0.1$. The fluid in cell 2 is conduction-dominated for the relatively slow motion. Two Ekman boundary layers form near the disk walls and, outside the layers, there appears a non-rotating core region where the fluid moves radially inward. Since the flow temperature in the core region lies at the temperature close to T_2, the thermal boundary layer on the disk 1 is thinner than that on the disk 2. Relatively, the faster-moving flow in cell 1 is convection-dominated. For $B < 0$, the buoyancy effects, assisting or opposing, on the two walls are reversed, the roles of two cells interchange. At the higher Reynolds number, $Re = 2000$ in Fig. 4(c), the above characteristic features become more noticeable.

Rotor–stator system of $\Omega_1 \neq \Omega_2 \equiv 0$ ($\gamma = -1$). Effects of centrifugal buoyancy on the velocity and temperature fields in a rotor–stator system are shown in Fig. 5. For $Re = 100$ in Fig. 5(a), the fluid adjacent

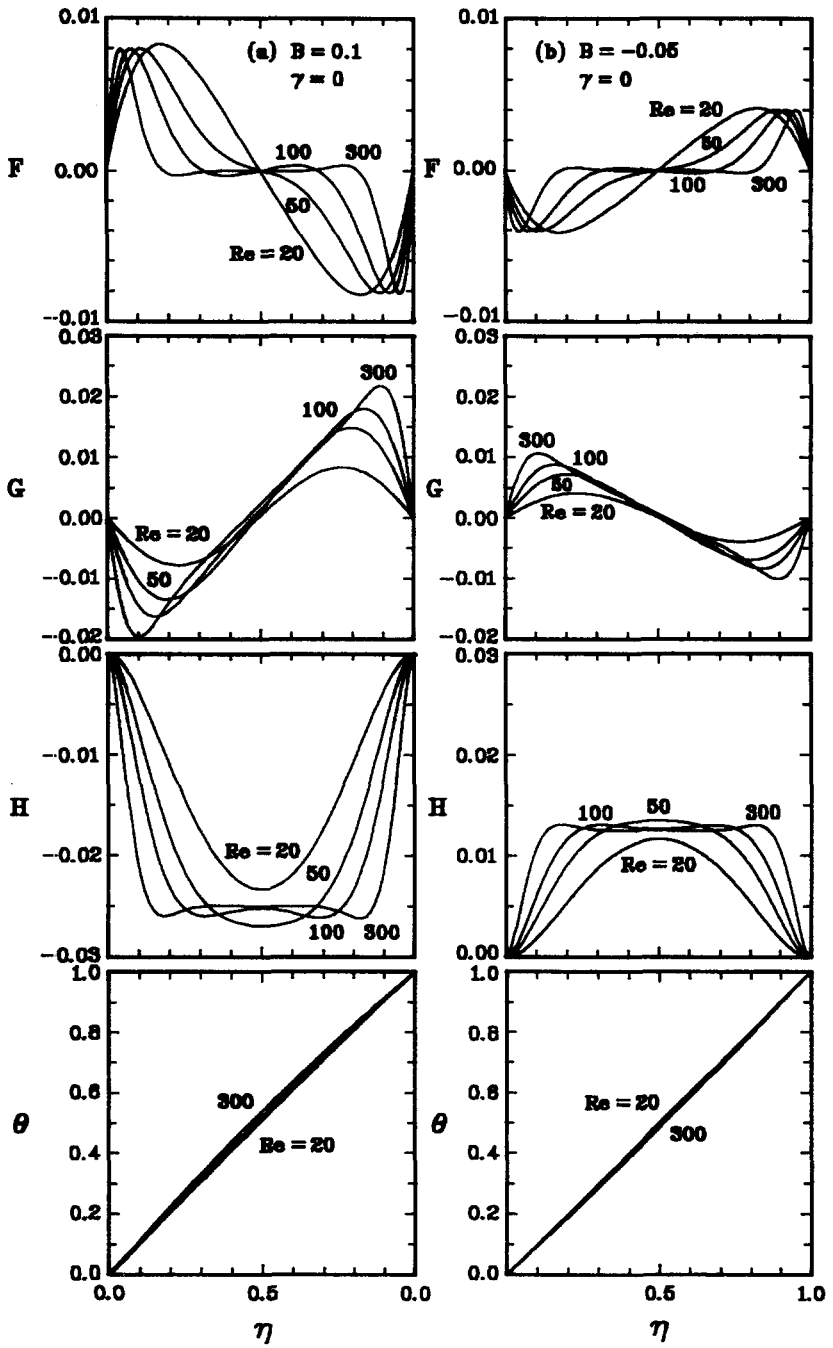

Fig. 3. Velocity and temperature solutions of co-rotating disks with $\gamma = 0$. (a) $B = 0.1$ and (b) $B = -0.05$.

to the rotating disk is pumped radially outward and the fluid near the stationary disk is sucked radially inwards as well as axially towards the rotating disk. As the buoyancy effect is present, e.g. $B = 0.1$, the cooler fluid near the rotating disk can be accelerated by the buoyancy-assisting effect; and the reverse situation appears near the stator. The more pumped fluid presents, the larger the negative axial velocity is. The most interesting feature is the variation of the circumferential velocity G, which is not a simply monotonic function. The slowly rotating fluid near the stator moves towards the rotor as well as radially inward. Therefore, as the fluid migrates to the location of, say, $\eta = 0.7$, the smaller R causes a larger rotational rate due to the conservation of angular momentum, see Fig. 5(a). As the fluid moves continuously to the location of $\eta = 0.3$, the radially outward motion leads to an increase in R as well as a decrease in rotational rate. However, in the proximity of the fast rotating disk ($\eta < 0.2$), the Coriolis and viscous effects dominate the momentum exchange based on the aforementioned procedure and the cir-

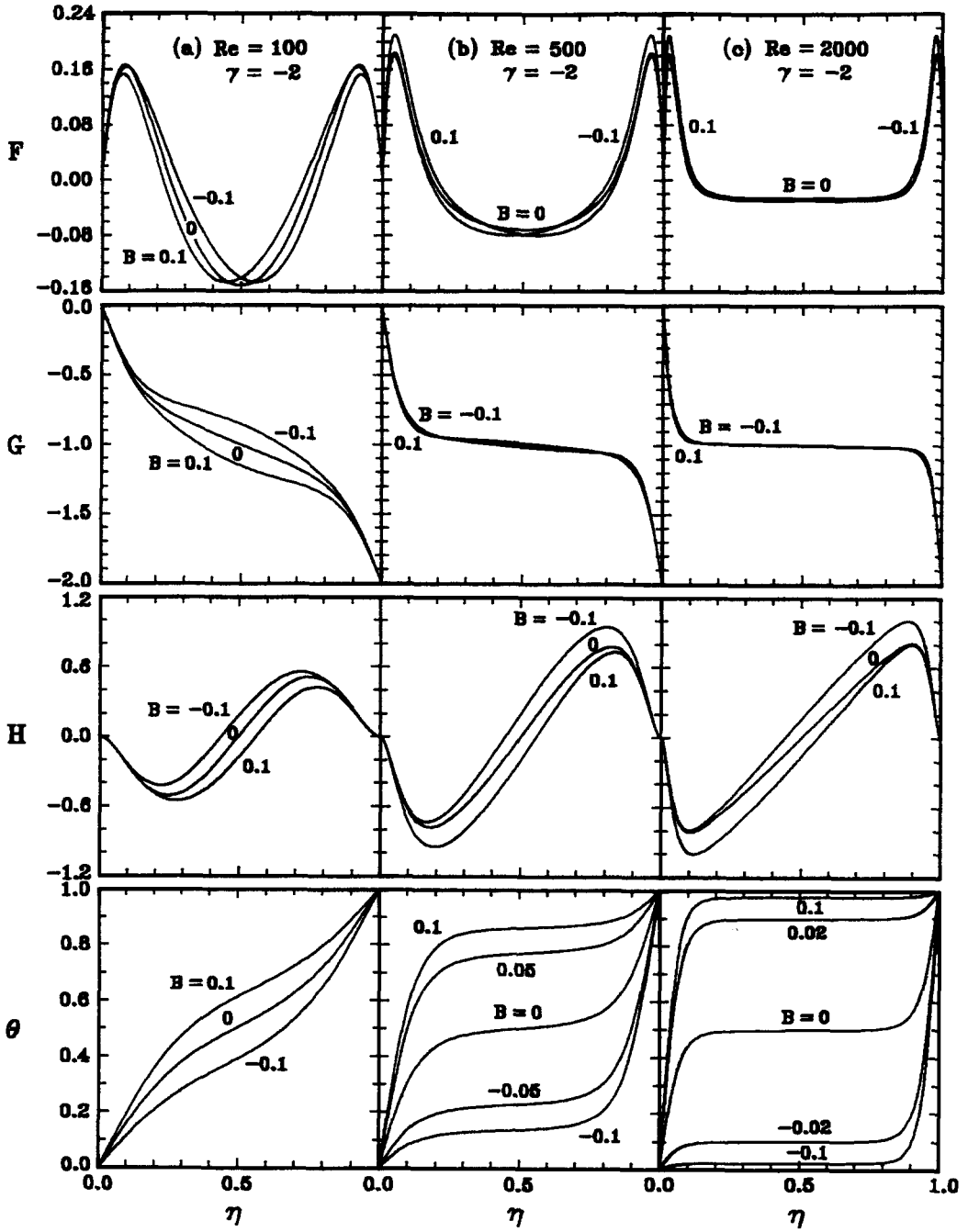

Fig. 4. Velocity and temperature solutions of counter-rotating disks with $\gamma = -2$. (a) $Re = 100$, (b) $Re = 500$, (c) $Re = 2000$.

cumferential velocity presents a peak value as well as the high gradients. In case $B < 0$ or $T_2 < T_1$, the interpretation of $B = -0.1$ solution follows the same philosophy.

For the case of $Re = 500$, in Fig. 5(b), the fluid adjacent to the stator lies approximately at the same temperature as the disk wall, but a thermal boundary layer forms at the rotating disk. From the radial velocity solution of $B = 0$, an inviscid core with almost constant rotational rate emerges. Due to the buoyancy-assisting effect at $B = 0.1$, the radial velocity near the rotor (cool disk) increases while that near the stator (hot disk) decreases, and it results in a larger axial velocity H. Therefore, more fluid at slow rotating rate near the stator moves towards the rotating center. For the conservation of angular momentum, the higher rotational rate can be resulted around $\eta = 0.8$ due to the rapid decrease in radial distance R. In

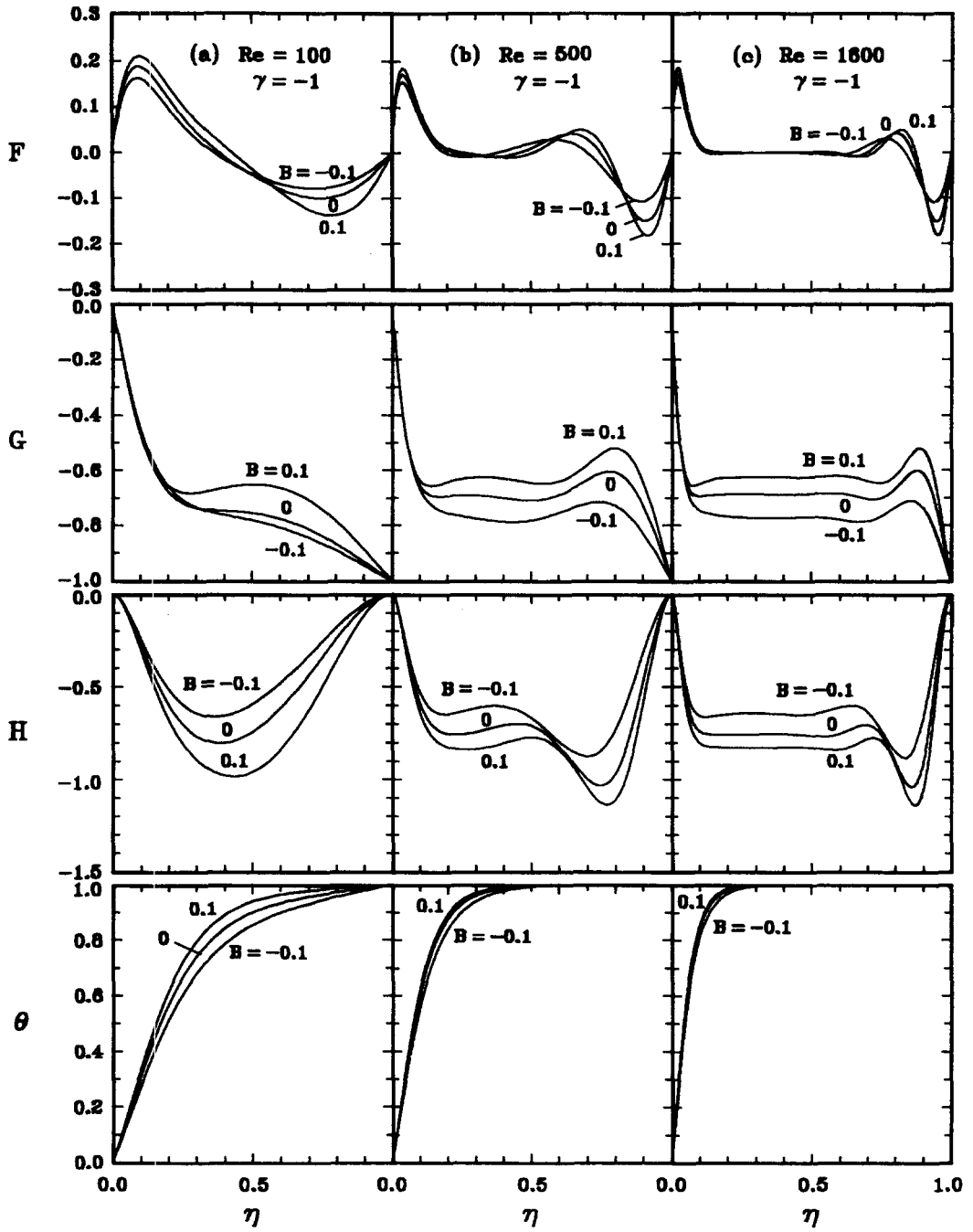

Fig. 5. Velocity and temperature solutions of rotor–stator system of $\gamma = -1$. (a) $Re = 100$, (b) $Re = 500$, (c) $Re = 1600$.

another aspect, this faster-rotating fluid may encounter a large centrifugal and Coriolis forces which push the fluid radially outward and make it lose the angular speed as moving axially, see F and G in the region of $0.5 < \eta < 0.8$ in Fig. 5(b). As for the core region, the fluid is nearly radially stationary and rotates at an almost constant rate.

As Re increases to a higher value, e.g. $Re = 1600$ in Fig. 5(c), the flow and temperature fields show the same trend as that at $Re = 500$ except the thinner Ekman and thermal boundary layers near the rotating disk and the larger as well as flatter core region. By inspecting the solutions at high Re, it is observed that the noticeable temperature gradient appears in the thermal boundary layer and the centrifugal buoyancy presents only small effects on the temperature and radial velocity distributions. However, the tangential and axial velocity can be indirectly but significantly

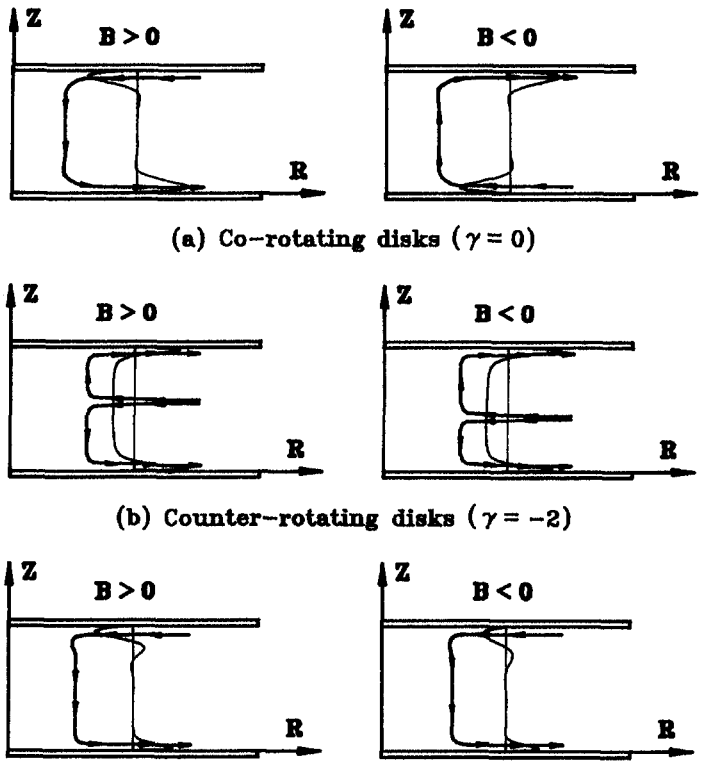

Fig. 6. Centrifugal-buoyancy effects on flow structure in R–Z plane. (a) Co-rotating disks, (b) counter-rotating disks, (c) rotor–stator system.

altered by buoyancy through the complicated mechanisms of momentum exchange. Note that the remarkable buoyancy effect on velocity fields appears even in the region of $\eta > 0.4$ where the fluid is almost isothermal.

Centrifugal-buoyancy effects on the flow structures in R–Z plane for co-rotating ($\gamma = 0$), counter-rotating ($\gamma = -2$) and rotor–stator ($\gamma = -1$) systems are summarized in Figs 6(a), (b) and (c), respectively. The thin curves in Fig. 6 denote radial velocity distribution $F(\eta)$ with a vertical line as the base of $F = 0$. The bold lines with arrows are the streamlines describing R–Z flow structures. Under the influence of the rotation-induced buoyancy, change in sign of the parameter B reverses the flow direction in the case of co-rotating disks with $\gamma = 0$. For the two-cell flow structure in counter-rotating disks, the buoyancy effects for positive and negative values of B are reflected in the interchange of the strengths of the two cells. Both of the above two cases present a symmetric nature of the flow field (see Appendix). In rotor–stator case ($\gamma = -1$), the centrifugal-buoyancy seems to have only insignificant influence on the flow structure.

Boundary layers and core solutions at high Reynolds numbers

In high-Re cases, the velocity and temperature distributions present the high-gradient layers near the rotating disks. For the quantitative analysis, herein, the location of the radial velocity peak near disk 1 is designated as the thickness of Ekman layer δ_E/S. In co-rotating disks for cases of $Re < 500$ considered, Ekman layers emerge on the two disks; but, for the small change in temperature field from the conduction state, no thermal boundary layer appears. Variation of δ_E/S with Re is shown in Fig. 7(a) and, obviously, buoyancy effect on the Ekman layer is negligibly small. The Ekman layer thickness in this situation can be well correlated as

$$\delta_E/S = 0.782 Re^{-0.5}. \tag{20}$$

For the rotor–stator and counter-rotating systems, the flow mechanisms are rather different from the free-convection flow in co-rotating disks. Correlation of the Ekman layer thickness for $\gamma = -1$ is formulated as

$$\delta_E/S = 0.923 Re^{-0.5} \tag{21a}$$

in which buoyancy effect is insignificant. In the case of the counter-rotating disks, the prediction of the correlation equation (21a) is surprisingly good at least in the range of $150 \leqslant Re \leqslant 3000$, see Fig. 7(b). However, the influences of buoyancy on the thermal boundary layer can not be ignored. Upon considering the location of $\theta = 0.999$ as the thermal boundary

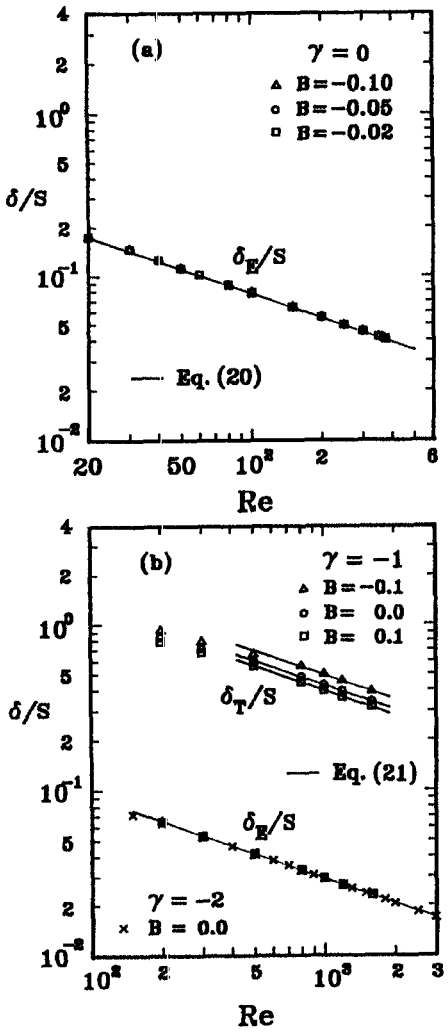

Fig. 7. Ekman and thermal boundary-layer thicknesses: (a) $\gamma = 0$ and (b) $\gamma = -1$ and -2.

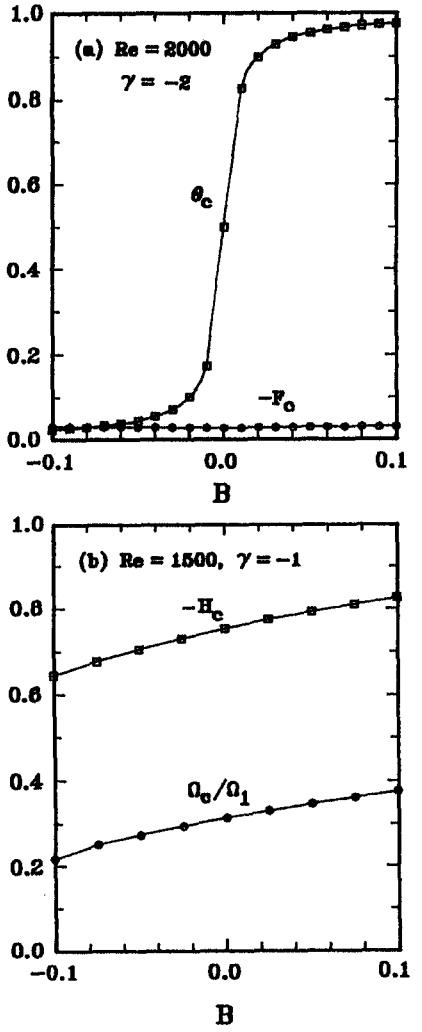

Fig. 8. Centrifugal buoyancy effects on core flow properties at high Reynolds numbers (a) counter-rotating disks at $Re = 2000$, (b) rotor–stator system at $Re = 1500$.

layer thickness δ_T/S in rotor–stator solutions, the values of δ_T/S at various conditions are plotted in Fig. 7(b). At the relatively higher Reynolds numbers, $Re > 500$, δ_T/S can be correlated as the following formula:

$$\delta_T/S = 13.635(1+4.984B)^{-0.202}\, Re^{-0.5}. \quad (21b)$$

Note that the thickness of the Ekman and thermal boundary layers are both proportional to $Re^{-0.5}$ just like the results of asymptotic analysis.

In the high-Re cases, as in the aforementioned field solutions, a core region emerges. Different core solution behaviors can be observed for various rotational conditions. From high-Re solutions, in the counter-rotating case, Fig. 4(c), it is found that the core solution, i.e. θ_c = constant, $G_c = -1$ and H_c is a linear function, can be categorized as that of equation (19a). In the rotor–stator system, see Fig. 5(c), the fluid in the core region possess zero radial velocity, and uniform tangential and axial velocities. The fluid temperature is nearly the same as the disk 2 except that in the thin thermal boundary layer. Obviously, the high-Re core solution for $\gamma = -1$ is exactly the category in equation (19b). The characteristic features of the core flow in a counter-rotating system at $Re = 2000$ are shown in Fig. 8(a). As shown in Fig. 4, it is reasonable to characterize the core flow temperature θ_c and radial velocity F_c at $\eta = 0.5$. The former, θ_c, is strongly influenced by the buoyancy effect, while the effect on the latter, F_c, is diminished in the high-Re cases. For $\gamma = -1$ and $Re = 1500$, Fig. 8(b) shows the representative core rotation rate Ω_c/Ω_1 and the axial velocity H_c at $\eta = 0.35$, in which it is believed that the asymptotic natures have appeared. It is noteworthy that, in Fig. 8(b), both the core rotation rate and the axial velocity are strongly affected by the buoyancy effects. Additionally, in an asymptotic sense of equation (8), the dimensionless pressure function ϕ is diminished as $Re \to \infty$.

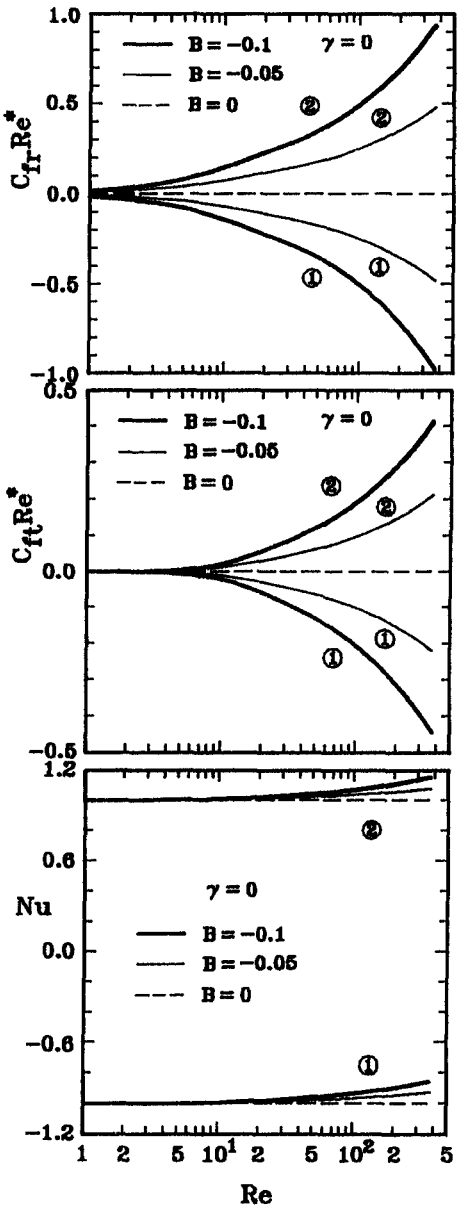

Fig. 9. Friction factors and heat transfer rates for co-rotating disks ($\gamma = 0$). The circled numbers 1 and 2 denote the disks 1 and 2, respectively.

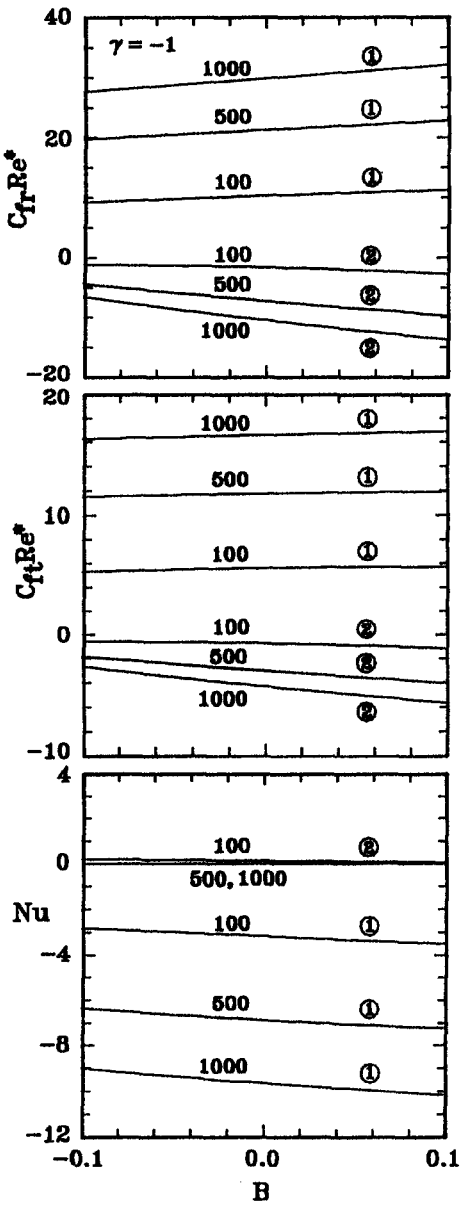

Fig. 10. Friction factors and heat transfer rates for rotor–stator systems ($\gamma = -1$). The circled numbers 1 and 2 denote the disks 1 and 2, respectively.

Friction factors and heat transfer rates

Friction factors and heat transfer rates for the cases of $\gamma = 0$, -1 and -2 are shown in Figs 9–11, respectively. For co-rotating disks ($\gamma = 0$) with $B = 0$ in Fig. 9, the radial and tangential friction factors are both zero and $Nu = \pm 1$ (conduction state) at two disks. For $B \neq 0$, increasing Re and B both enhance buoyancy effects on friction factors and heat transfer rates. In the rotor–stator system, the values of $C_{fr}Re^*$, $C_{ft}Re^*$ and Nu are nearly linearly varying with B, see Fig. 10. Generally speaking, they are not strongly influenced by the centrifugal buoyancy; however, at high Re, the buoyancy effect may become more important for friction factors at disk 2. For counter-rotating disks of $\gamma = -2$, Fig. 11 indicates that the friction factors and heat transfer rates are significantly affected by the centrifugal buoyancy. Particularly, due to the strong influence of buoyancy on the temperature fields in this two-cell flow structure, the variations in Nusselt numbers are most striking. In the high-Re case of $Re = 1000$, the influences of the buoyancy effect increase, at least on the radial friction factor $C_{fr}Re^*$ and Nusselt number Nu.

Physically, the heat transfer through two disk walls

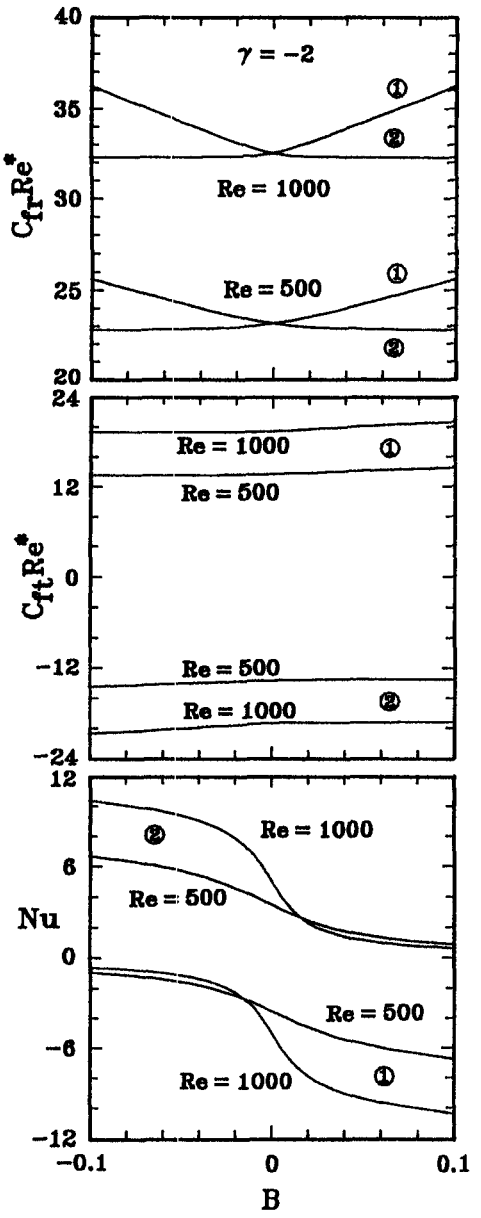

Fig. 11. Friction factors and heat transfer rates for counter-rotating disks ($\gamma = -2$). The circled numbers 1 and 2 denote the disks 1 and 2, respectively.

are not in balance. The fluid enthalpy change in the radial flow process of sucked inward and then pumped outward motion must be included. Mathematically, integrating the energy equation (6) in the region of $0 \leqslant \eta \leqslant 1$ and introducing the continuity equation (7) leads to

$$\theta'(1) - \theta'(0) = 2Pr\,Re \int_0^1 F\theta \,\mathrm{d}\eta \qquad (22)$$

where the integral, which stands for a net enthalpy change of the radial flow, is not necessarily zero and, therefore, $\theta'(1) \neq \theta'(0)$ in general. In Figs 10 and 11, for example, the values of $Nu_1 + Nu_2$, i.e. $\theta'(0) - \theta'(1)$, are not zero and may become remarkable for large Re.

CONCLUDING REMARKS

A similarity analysis for rotation-induced forced, free and mixed convection in non-isothermal flows between coaxial infinite disks has been developed. Through the present theoretical model, the non-isothermal flow behaviors in the presence of centrifugal buoyancy can be explored in detail, and the following conclusions can be drawn:

(1) The centrifugal-buoyancy is a significant effect on the flow and heat transfer characteristics of this class of rotating disk problems. Although the parameters Re and B can be used to characterize the forced (for $\gamma \neq 0$) and free convection effects, unlike that in the conventional mixed convection in gravitational force field, however, as Re increases the buoyancy effect can still survive and even grow rather than diminish in some circumstances. It is attributed to the special coupling of forced and buoyancy-induced flows in this problem. The forced flow is caused by the rotation-induced pumping effect. Raising the rotational rate to increase the forced flow (Re) effect can also lead to an enhancement in the centrifugal-buoyancy.

(2) The centrifugal-buoyancy effects on velocity and temperature fields are quite different in various rotational conditions. In co-rotating disks with $\gamma = 0$, the centrifugal buoyancy induces a buoyant flow and plays a role as the buoyancy in conventional free convection. In a counter-rotating system of $\gamma = -2$, the most striking influences of the buoyancy are those on the temperature field and heat transfer rates. Also, noticeable effects on the two-cell flow structure including radial and axial velocities and the location of the DSS can be observed. In rotor–stator systems, especially at high Reynolds numbers, the major effects of buoyancy appear on the rotating core in the off-wall region. In this situation, the buoyancy effects on the boundary parameters, i.e. the friction factors and heat transfer rates, are relatively small.

(3) High-gradient layers appear on the rotating walls at sufficiently high Re. Generally, the Ekman layer thicknesses are of order $Re^{-1/2}$ for various rotational conditions and not significantly affected by the centrifugal buoyancy at least for the buoyancy parameter of $|B| \leqslant 0.1$ in this study. No thermal boundary layer emerges on co-rotating disks at $Re < 500$. For rotor–stator systems, thermal boundary layer thickness is also proportional to $Re^{-1/2}$, but, on it the buoyancy effect can not be ignored. Correlations for thicknesses of the Ekman and thermal boundary layers for $\gamma = 0$, -1 and -2 are proposed.

(4) In a complex nonlinear dynamic system like this, solution multiplicity and bifurcation nature are significant. A study of nonlinearity is beyond the scope

of the present work; however, it is useful to further the understanding of the present flow configuration and is a worthwhile study.

REFERENCES

1. T. von Karman, Laminar und turbulente reibung, *Z. Angew. Math. Mech.* **1,** 233–244 (1921).
2. G. K. Batchelor, Note on a class of solutions of the Navier–Stokes equations representing steady rotationally-symmetric flow, *Quart. J. Mech. Appl., Marh.* **IV,** 29–41 (1951).
3. K. Stewartson, On the flow between two rotating coaxial disks, *Proc. Camb. Phil. Soc.* **3,** 333–341 (1953).
4. G. N. Lance and M. H. Rogers, The axially symmetric flow of a viscous fluid between two infinite rotating disks, *Proc. R. Sci. A* **266,** 109–121 (1962).
5. C. E. Pearson, Numerical solutions for the time-dependent viscous flow between two rotating coaxial disks, *J. Fluid Mech.* **21,** 623–633 (1965).
6. G. L. Mellor, P. J. Chapple and V. K. Stokes, On the flow between a rotating and a stationary disk, *J. Fluid Mech.* **31,** 95–112 (1968).
7. A. Z. Szeri, S. J. Schneider, F. Labbe and H. N. Kaufman, Flow between rotating disks—I. Basic flow, *J. Fluid Mech.* **134,** 103–131 (1983).
8. D. Dijkstra and G. J. F. van Heijsst, The flow between two finite rotating disks enclosed by a cylinder, *J. Fluid Mech.* **128,** 123–154 (1983).
9. S. M. Roberts and J. S. Shipman, Computation of the flow between a rotating and a stationary disk, *J. Fluid Mech.* **73,** 53–63 (1976).
10. K. E. Barrett, Numerical study of the flow between rotating coaxial discs, *Z. Angew. Math. Mech.* **26,** 807–816 (1975).
11. F. H. Busse and C. R. Carrigan, Convection induced by centrifugal buoyancy, *J. Fluid Mech.* **62,** 579–592 (1974).
12. G. M. Homsy and J. L. Hudson, Centrifugally driven thermal convection in a rotating cylinder, *J. Fluid Mech.* **35,** 33–52 (1969).
13. G. M. Homsy and J. L. Hudson, Heat transfer in a rotating cylinder of fluid heated from above, *Int. J. Heat Mass Transfer* **14,** 1149–1159 (1971).
14. J. L. Hudson, D. Tang and S. Abell, Experiments on centrifugally driven thermal convection in a rotating cylinder, *J. Fluid Mech.* **86,** 147–159 (1978).
15. J. Y. Guo and C. M. Zhang, Thermal drive in centrifugally driven thermal convection in a vertical rotating cylinder, *Int. J. Heat Mass Transfer* **35,** 1635–1644 (1992).
16. T. Matsuda and K. Hashimoto, Thermally, mechanically or externally driven flows in a gas centrifuge with insulated horizontal end plates, *J. Fluid Mech.* **78,** 337–354 (1976).
17. T. Matsuda, K. Hashimoto and H. Takeda, Thermally driven flow in a gas centrifuge with an insulated side wall, *J. Fluid Mech.* **73,** 389–399 (1976).
18. R. Siegel, Analysis of buoyancy effect on fully developed laminar heat transfer in a rotating tube, *J. Heat Transfer* **107,** 338–344 (1985).
19. C. Y. Soong and G. J. Hwang, Laminar mixed convection in a radially rotating semiporous channel, *Int. J. Heat Mass Transfer* **33,** 1805–1816 (1990).
20. C. Y. Soong and G. J. Hwang, Stress work effects on similarity solutions of mixed convection in rotating channels with wall-transpiration, *Int. J. Heat Mass Transfer* **36,** 845–856 (1993).
21. C. Y. Soong and W. M. Yan, Numerical study of mixed convection between two symmetrically-heated corotating disks, *AIAA J. Thermophys. Heat Transfer* **7,** 165–170 (1993).
22. C. Y. Soong and W. M. Yan, Transport phenomena in non-isothermal flow between co-rotating asymmetrically-heated disks, *Int. J. Heat Mass Transfer* **37,** 2221–2230 (1994).
23. C. Y. Soong and R. Y. Tzong, Numerical investigation of non-isothermal flow in a shrouded rotor–stator system, Paper presented at the 33rd Aeronautics Astronautics Conference, AASRC, Taipei, Taiwan, R.O.C. (1991).
24. J. L. Hudson, Non-isothermal flow between rotating disks, *Chem. Engng Sci.* **23,** 1007–1020 (1968).
25. J. W. Chew, Similarity solutions for non-isothermal flow between infinite rotating disks, Report TFMRC/38, Thermo-Fluid Mechanics Research Centre, School of Engineering and Applied Science, University of Sussex (1981).
26. C. Y. Soong and H. L. Ma, Unsteady analysis of non-isothermal flow and heat transfer between rotating coaxial disks, *Int. J. Heat Mass Transfer* **38,** 1865–1878 (1995).
27. C. Y. Soong and C. H. Chyuan, A similarity solution of rotation induced mixed convection between rotating coaxial disks, Paper presented at the Fifteenth National Conference on Theoretical and Applied Mechanics, Tainan, Taiwan, R.O.C. (1991).
28. J. M Owen and R. H. Rogers, *Flow and Heat Transfer in Rotating-Disc Systems*, Vol. 1, *Rotor–Stator Systems*. Research Studies Press Ltd, Somerset, U.K. (1989).
29. S. Mochizuki, Unsteady flow and heat transfer in rotating-disk systems. In *Transport Phenomena in Thermal Engineering*, Vol. 2 (edited by J. S. Lee, S. H. Chung and K. H. Kim), pp. 1265–1275. Begell House, U.S.A. (1993).
30. K. Stewartson, C. J. Simpson and R. J. Bodonyi, The unsteady laminar boundary layer on a rotating disk in a counter-rotating fluid—II, *J. Fluid Mech.* **121,** 507–515 (1982).
31. P. Singh, P. Radhakrishnan and K. A. Narayan, Fluctuating flow due to unsteady rotation of a disk, *AIAA J.* **27**(2), 150–154 (1989).
32. B. G. Higgins, Film flow on a rotating disk, *Phys. Fluids* **29**(11), 3522–3529 (1986).
33. T. J. Rehg and B. G. Higgins, The effects of inertial and interfacial shear on film flow on a rotating disk, *Phys. Fluids* **31**(6), 1360–1371 (1988).
34. D. D. Gray and A. Giorgini, The validity of the Boussinesq approximation for liquid and gases, *Int. J. Heat Mass Transfer* **19,** 545–551 (1976).
35. J. A. D. Ackroyd, Stress work effects in laminar flat-plate natural convection, *J. Fluid Mech.* **62,** 677–695 (1974).
36. J. D. Cole, *Perturbation Methods in Applied Mathematics*. Blaisdell, Walttham (1968).
37. H. B. Keller and R. K.-H. Szeto, Calculation of flow between rotating disks. In *Computing Methods in Applied Sciences and Engineering* (Edited by R. Glowinski and J. L. Lions). North-Holland, INRIA (1980).
38. C. Vaughan, A numerical investigation into the effect of an external flow field on the sealing of a rotor–stator cavity, Ph.D. Thesis, University of Sussex, U.K. (1986).
39. A. S. Sambo, A theoretical and experimental study of the flow between a rotating and a stationary disc, Ph.D. Thesis, University of Sussex, U.K. (1983).
40. M. Itoh, Y. Yamada and K. Nishioka, Experimental study on flow transition due to rotating disk in an enclosure, *J. JSME, ser. B* **51**(462), 452–460 (1985) [in Japanese].

APPENDIX

Symmetry of non-isothermal flow solutions in two-disk problems

From the analytic characteristics of the problem, each solution with $|1+\gamma| \leqslant 1$, but except $\gamma = -1$, has a cor-

responding solution with $|1+\gamma| \geqslant 1$. The situation is just equivalent to interchanging the roles of the two disks. For non-isothermal flows with heat convection and centrifugal buoyancy, the lemma for solution symmetry proposed by Keller and Szeto [37] has to be modified in terms of the present nomenclature.

Lemma: Let the system of the equations (4)–(6) and boundary conditions (9) with $\gamma \neq 1$ have a solution set $\mathscr{I}$.

$$\mathscr{I} = [\mathrm{H}(\eta), \mathrm{G}(\eta), \theta(\eta), \mathrm{Re}, \mathrm{B}, \gamma, \text{ on } 0 \leqslant \eta \leqslant 1]$$

then a conjugate solution set $\hat{\mathscr{I}}$ is given by

$$\hat{\mathscr{I}} = [\hat{\mathrm{H}}(\zeta), \hat{\mathrm{G}}(\zeta), \hat{\theta}(\zeta), \hat{\mathrm{Re}}, \hat{\mathrm{B}}, \hat{\gamma}, \text{ on } 0 \leqslant \zeta \leqslant 1]$$

where

$$\hat{H}(\zeta) \equiv -H(\eta)/\sqrt{(|+\gamma|)}, \quad \hat{G}(\zeta) \equiv [G(\eta)-\gamma]/(1+\gamma)$$

$$\hat{\theta} \equiv 1-\theta(\eta) \quad \zeta \equiv 1-\eta, \quad \hat{Re} \equiv |1+\gamma|Re$$

$$\hat{B} \equiv -B/(1+\gamma)^2, \quad \hat{\gamma} \equiv -\gamma/(1+\gamma). \tag{A1}$$

According to the symmetric nature, without actually computing it, each conjugate solution in $\hat{\mathscr{I}}$ can be found by directly converting its counterpart in $\mathscr{I}$ using the transformation in equation (A1). This analytic transformation can be used to check numerical solutions.